Unraveling Self-Similar Energy Transfer Dynamics: a Case Study for 1D Burgers System

Pritpal Matharu*[1,2], Bartosz Protas[3], and Tsuyoshi Yoneda[4]

[1]Max Planck Institute for Mathematics in the Sciences, Leipzig, Germany
[2]Department of Mathematics, KTH Royal Institute of Technology, Stockholm, Sweden
[3]Department of Mathematics and Statistics, McMaster University, Hamilton, Ontario, Canada
[4]Graduate School of Economics, Hitotsubashi University, Tokyo, Japan

July 18, 2025

Abstract

In this work we consider the problem of constructing flow evolutions leading to a self-similar energy cascade consistent with Kolmogorov's statistical theory of turbulence. As a first step in this direction, we focus on the one-dimensional viscous Burgers equation as a toy model. Its solutions exhibiting self-similar behavior, in a precisely-defined sense, are found by framing this problems in terms of PDE-constrained optimization. The main physical parameters are the time window over which self-similar behavior is sought (equal to approximately one eddy turnover time), viscosity (inversely

*Email address for correspondence: `matharu@mis.mpg.de`

proportional to the "Reynolds number") and an integer parameter characterizing the distance in the Fourier space over which self-similar interactions occur. Local solutions to this nonconvex PDE optimization problems are obtained with a state-of-the-art adjoint-based gradient method. Two distinct families of solutions, termed *viscous* and *inertial*, are identified and are distinguished primarily by the behavior of enstrophy which, respectively, uniformly decays and grows in the two cases. The physically meaningful and appropriately self-similar inertial solutions are found only when a sufficiently small viscosity is considered. These flows achieve the self-similar behaviour by a uniform steepening of the wave fronts present in the solutions. The methodology proposed and the results obtained represent an encouraging proof of concept for this approach to be employed to systematically search for self-similar flow evolutions in the context of three-dimensional turbulence.

Keywords: Turbulence; Self-Similar Energy Cascade; 1D Viscous Burgers Equation; PDE-constrained Optimization

1 Introduction

Self-similarity of the energy cascade is one of the most prominent statistical properties of hydrodynamic turbulence [Frisch, 1995]. The energy cascade between a hierarchy of spatial and temporal scales was described first by Richardson [Richardson, 1922], who provided a statistical account of this cascade in turbulent flows. This idea further leads to the concept of self-similar flow structures predicted by Kolmogorov [Kolmogorov, 1941] who proposed a similarity hypothesis to explain the -5/3 power law describing the energy cascade. However, this approach is based on dimensional analysis of quantities defined in statistical terms and therefore is not directly related to the mathematical structure of the solutions of the Navier-Stokes system. In other words, being statistical in nature, this theory does not offer any insights into what kind of fluid motions can generate an energy cascade with the spectrum characterized by the -5/3 power law.

In 2017, Goto, Saito & Kawahara [Goto *et al.*, 2017] used direct numerical simulation (DNS) to reveal that the 3D Navier-Stokes turbulence in a periodic box has a hierarchical structure consisting of vortex tubes with a range of characteristic length scales. At each of these scales, the vortex tubes generate a strain field that contributes to the generation of smaller-scale vortex tubes. Based on that result, Yoneda, Goto & Tsurhashi [Yoneda *et al.*, 2022] reformulated Kolmogorov's -5/3 power law by defining an energy-transfer function in terms of vorticity [Yoneda

2

et al., 2022, equation (2.6)] and then using it to identify a clear local-in-scale energy transfer structure from instantaneous spatially-averaged turbulence snapshots [Yoneda *et al.*, 2022, Figure 1],[Tsuruhashi *et al.*, 2022]. However, that approach was based on spatial averaging and therefore it was not possible to identify the elementary processes, in the form of specific flow evolutions in time, that give rise to a self-similar energy cascade. The purpose of this study is to address this question in the context of a simple toy model of turbulent flows, namely, the one-dimensional (1D) Burgers equation. A key novelty of our approach is that solutions with a certain self-similar structure are sought systematically by solving suitably-defined optimization problems for a partial differential equation (PDE). By focusing on a simplified model problem we aim to develop an approach that will provide a proof of concept that would then serve as a stepping stone on the way to the study of analogous self-similar flow evolutions in the context of the 3D turbulence.

While PDE-constrained optimization has had a long history in fluid mechanics [Gunzburger, 2003], most of these studies have focused on solution of practical problems often motivated by engineering applications [Jameson, 1988, Bewley *et al.*, 2001, Matharu and Protas, 2020, 2022]. It was only recently that such techniques were employed to investigate fundamental questions concerning the structure and properties of solutions to hydrodynamic equations in a way that complements rigorous mathematical analysis [Protas, 2022]. Problems tackled in this way include probing sharpness of a priori bounds on various energy-type quantities [Ayala and Protas, 2011, Ayala *et al.*, 2018], nonlinear stability [Kerswell *et al.*, 2014], dissipation anomaly [Matharu *et al.*, 2022], search for finite time singularities [Ayala and Protas, 2017, Kang *et al.*, 2020, Kang and Protas, 2021, Zhao and Protas, 2023] and optimization of mixing [Hassanzadeh *et al.*, 2014, Miles and Doering, 2018]. The present study builds on this line of research.

The main goal of this work is to find and analyze a family of 1D Burgers flows featuring a self-similar energy cascade and parametrized by the value of the viscosity coefficient (or, equivalently, the Reynolds number) and a positive integer number characterizing the nonlocality of interactions in the Fourier space. The initial conditions for these flows are found as solutions of PDE-constrained optimization problems and are obtained numerically using a state-of-the-art adjoint-based optimization method. Our main finding is the evidence that families of such Burgers flows do indeed exist and that their self-similar behavior is realized by a uniform steepening of the fronts in the solutions. We also provide an analysis of how quantitative details of this process depend on physical parameters.

The structure of the paper is as follows: in the next section we introduce the

model and state the optimization problem; in Section 3 we describe the solution approach whereas the results are presented in Section 4; discussion and final conclusions are deferred to Section 5 while some technical material is collected in an appendix.

2 The Governing Equation and Optimization Formulation

In this section we first introduce the 1D Burgers system and briefly discuss some properties of its solutions. It will be considered on the periodic domain $\Omega = \mathbb{T} := [0, 2\pi]$ and over the time window $[0, T]$, where the choice of the end time T will be discussed below. Then, we formulate a PDE optimization problem designed to find solutions exhibiting a self-similar evolution.

2.1 1D Burgers Equation

The Burgers system in 1D has the following form subject to the periodic boundary conditions

$$\frac{\partial u}{\partial t} + u \frac{\partial u}{\partial x} - \nu \frac{\partial^2 u}{\partial x^2} = 0 \qquad \text{in } (0, T] \times \Omega, \tag{1a}$$

$$u(t = 0) = \phi \qquad \text{in } \Omega, \tag{1b}$$

where $\nu > 0$ is the viscosity and ϕ is the initial condition. It is known to admit globally defined smooth solutions for a broad class of initial data ϕ [Kreiss and Lorenz, 2004]. Anticipating the formulation of the optimization problem below, we will assume here that $\phi \in H^1(\Omega)$, where $H^1(\Omega)$ is the Sobolev space of functions with square-integrable weak derivatives endowed with the inner product [Adams, 2003]

$$\langle p_1, p_2 \rangle_{H^1(\Omega)} := \int_\Omega p_1 p_2 + \ell^2 \left(\frac{\partial p_1}{\partial x} \frac{\partial p_2}{\partial x} \right) \, dx, \qquad \forall \, p_1, p_2 \in H^1(\Omega), \tag{2}$$

where ":=" means "equal to by definition" and $0 < \ell < \infty$ is an adjustable parameter (its significance will become evident in Section 3).

Various stochastic variants of system (1) have been used as models of turbulence [Bec and Khanin, 2007]. On a phenomenological level, equation (1a) describes the competition between a nonlinear amplification in the form of wave steepening,

4

which represents the forward energy cascade with energy transferred from large to small scales, and viscous dissipation [Fournier and Frisch, 1983]. The wave steepening is characterized by the evolution of the enstrophy

$$\mathcal{E}(u(t,\cdot)) := \int_0^{2\pi} \left| \frac{\partial u(t,x)}{\partial x} \right|^2 \, dx = \|u(t,\cdot)\|_{\dot{H}^1}^2, \tag{3}$$

which is well understood [Ayala and Protas, 2011, Pelinovsky, 2012a,b]. In particular, sharp a priori bounds on the maximum growth of the enstrophy are now available [Albritton and Nitti, 2023]. The triadic interactions responsible for the amplification of the enstrophy in 1D Burgers flows were analyzed in [Murray and Bustamante, 2018, Buzzicotti *et al.*, 2016, Protas *et al.*, 2024].

2.2   Optimization Problem

Before we can state the optimization problem, we need to define a suitable notion of "self-similar evolution". Let $\widehat{u}(t,k)$, $k \in \mathbb{N}$, denote the Fourier coefficient of the solution $u(t,x)$ at some time $t \geq 0$. Given a positive integer $\lambda \in \mathbb{N}^+$, we have the following

Definition 1 *A solution $u = u(t,x)$ of* (1) *is said to be self-similar with an index λ in terms of spectral energy transfer on $[t, t+T]$ if it satisfies the relation*

$$|\widehat{u}(t,k)|^2 = \lambda \, |\widehat{u}(t+T, \lambda k)|^2, \qquad k \in \mathbb{N}, \quad t > 0. \tag{4}$$

For brevity, we will refer to solutions satisfying this definition as simply "self-similar". Intuitively, relation (4) can be interpreted to mean that during a self-similar evolution over the time T a fraction $(1/\lambda) \in (0,1)$ of the kinetic energy is transferred between the Fourier modes with wavenumbers k and λk. While existence of such solutions in a mathematically precise sense remains an open question, we will attempt here to construct them by finding initial conditions ϕ that minimize the functional $\mathcal{J}_{\nu,\lambda} : H^1(\Omega) \to \mathbb{R}$ defined as

$$\mathcal{J}_{\nu,\lambda}(\phi) := \frac{1}{2} \sum_{k=0}^{\infty} \underbrace{\left| |\widehat{\phi}(k)|^2 - \lambda|\widehat{u}(T, \lambda k; \phi)|^2 \right|^2}_{f(k;\phi)} \tag{5}$$

in which summation is restricted to positive wavenumbers k only due to the conjugate symmetry $\widehat{u}(\cdot,k) = \overline{\widehat{u}(\cdot,-k)}$, where the overbar denotes complex conjugation, characterizing the Fourier coefficients of real-valued functions.

Clearly, in the absence of any constraints, the global minimum of $\mathcal{J}_{\nu,\lambda}(\phi)$ is achieved by $\phi_0 \equiv 0$, since then $u(t; \phi_0) \equiv 0$, $t > 0$, and $\mathcal{J}_{\nu,\lambda}(\phi_0) = 0$. In order to avoid such uninteresting trivial solutions, we need to constrain the initial condition to have a nonvanishing magnitude and we choose to do this by prescribing its enstrophy as $\mathcal{E}(\phi) = \mathcal{E}_0 > 0$. We thus have the following optimization problem

Problem 1 *For fixed T, $\mathcal{E}_0, \nu \in \mathbb{R}^+$ and $\lambda \in \mathbb{N}^+$ in (5), find*

$$\varphi_{\nu,\lambda} = \arg\min_{\phi \in \mathcal{S}} \mathcal{J}_{\nu,\lambda}(\phi), \quad \text{where} \quad \mathcal{S} := \left\{ \phi \in H^1(\Omega) \; : \; \int_0^{2\pi} \phi(x)\, dx = 0, \quad \mathcal{E}(\phi) = \mathcal{E}_0 \right\}.$$

In the above $\mathcal{S} \subset H^1(\Omega)$ represents the constraint manifold which also includes the zero-mean condition (which is a property preserved in the evolution governed by (1a)). The time window T will be taken on the order of an eddy turnover time t_e defined as

$$t_e := \sqrt{\frac{\nu}{\varepsilon}}, \tag{6}$$

where ε the space-time averaged energy dissipation $\varepsilon := \frac{2\nu}{T|\Omega|} \int_0^T \mathcal{E}(u(t, \cdot))\, dt$.

3 Solution Approach

While methods of adjoint analysis are now well known [Gunzburger, 2003], we introduce our approach in some detail below given the somewhat nonstandard structure of the objective functional which is defined in the Fourier space (5). Problem 1 is Riemanian in the sense that its solutions are constrained to a Riemannian manifold $\mathcal{S} \subset H^1(\Omega)$ [Absil *et al.*, 2008]. It is also nonconvex and its local minimizers are approximated as $\varphi_{\nu,\lambda} = \lim_{n\to\infty} \phi^{(n)}$ using a retracted discrete gradient flow

$$\phi^{(n+1)} = \mathcal{R}_{\mathcal{S}} \left(\phi^{(n)} + \tau_n \nabla \mathcal{J}_{\nu,\lambda}\left(\phi^{(n)} \right) \right), \qquad n = 1, 2, \ldots,$$
$$\phi^{(1)} = \phi_1, \tag{7}$$

where $\phi^{(n)}$ is an approximation of the minimizer obtained at the n-th iteration, $\phi_1 \in \mathcal{S}$ is the initial guess, $\mathcal{R}_{\mathcal{S}} \; : \; H^1(\Omega) \to \mathcal{S}$ is the retraction operator defined below and τ_n is the length of the step in the direction of the gradient $\nabla \mathcal{J}_{\nu,\lambda}(\phi^{(n)})$. To exploit the mathematical structure of Problem 1, we will adopt

the "optimize-then-discretize" approach [Gunzburger, 2003] where expressions for the different elements in (7) are derived in the continuous setting and discretized for the purpose of numerical evaluation at the final stage only; these steps are documented in Section 3.1 below.

To obtain an expression for the gradient $\nabla \mathcal{J}_{\nu,\lambda}(\phi)$ of the objective functional $\mathcal{J}_{\nu,\lambda}(\phi)$, we begin by defining its Gâteaux (directional) differential $\mathcal{J}_{\nu,\lambda}'(\phi; \phi') := \lim_{\epsilon \to 0} \epsilon^{-1} \left[\mathcal{J}_{\nu,\lambda}(\phi + \epsilon \phi') - \mathcal{J}_{\nu,\lambda}(\phi) \right]$ for some arbitrary perturbation $\phi' \in H^1(\Omega)$ of the initial condition. Given the definition of the functional in (5), the Gâteaux differential is

$$
\begin{aligned}
\mathcal{J}_{\nu,\lambda}'(\phi; \phi') &= \sum_{k=0}^{\infty} \left[|\widehat{\phi}(k)|^2 - \lambda \, |\widehat{u}(T, \lambda k; \phi)|^2 \right] \, \left[\widehat{\phi'}(k) \overline{\widehat{\phi}}(k) + \widehat{\phi}(k) \overline{\widehat{\phi}'}(k) \right] \\
&\quad - \sum_{k=0}^{\infty} \lambda \left[|\widehat{\phi}(k)|^2 - \lambda \, |\widehat{u}(T, \lambda k; \phi)|^2 \right] \, \left[\widehat{u'}(T, \lambda k; \phi, \phi') \overline{\widehat{u}}(T, \lambda k; \phi) \right] \\
&\quad - \sum_{k=0}^{\infty} \lambda \left[|\widehat{\phi}(k)|^2 - \lambda \, |\widehat{u}(T, \lambda k; \phi)|^2 \right] \, \left[\widehat{u}(T, \lambda k; \phi) \overline{\widehat{u}'}(T, \lambda k; \phi, \phi') \right], \\
&= 2 \sum_{k=0}^{\infty} \left[|\widehat{\phi}(k)|^2 - \lambda \, |\widehat{u}(T, \lambda k; \phi)|^2 \right] \widehat{\phi}(k) \overline{\widehat{\phi}'}(k) \\
&\quad \underbrace{- 2 \sum_{k=0}^{\infty} \lambda \left[|\widehat{\phi}(k)|^2 - \lambda \, |\widehat{u}(T, \lambda k; \phi)|^2 \right] \widehat{u}(t, \lambda k; \phi) \overline{\widehat{u}'}(t, \lambda k; \phi, \phi')}_{\mathcal{A}(\phi; \phi')},
\end{aligned}
\tag{8}
$$

where we used the identity $\sum_{k=0}^{\infty} \widehat{v}_1(k) \overline{\widehat{v}}_2(k) = \sum_{k=0}^{\infty} \overline{\widehat{v}}_1(k) \widehat{v}_2(k)$ valid for real-valued functions $v_1(x)$, $v_2(x)$ and $u'(t, x; \phi, \phi')$ satisfies the perturbation system

$$
\frac{\partial u'}{\partial t} + u' \frac{\partial u}{\partial x} + u \frac{\partial u'}{\partial x} - \nu \frac{\partial^2 u'}{\partial x^2} = 0 \qquad \text{in } (0, T] \times \Omega, \tag{9a}
$$

$$
u'(t = 0) = \phi' \qquad \text{in } \Omega \tag{9b}
$$

obtained by linearizing system (1) around the solution $u(\cdot, \cdot; \phi)$. Noting that when viewed as a function of its second argument (ϕ') and for a fixed ϕ, the Gâteaux differential (8) is a bounded linear functional on both $H^1(\Omega)$ and $L^2(\Omega)$, and we can invoke the Riesz representation theorem [Berger, 1977]

$$
\mathcal{J}_{\nu,\lambda}'(\phi; \phi') = \left\langle \nabla^{H^1} \mathcal{J}_{\nu,\lambda}, \phi' \right\rangle_{H^1(\Omega)} = \left\langle \nabla^{L^2} \mathcal{J}_{\nu,\lambda}, \phi' \right\rangle_{L^2(\Omega)}, \tag{10}
$$

where the inner product $\langle \cdot, \cdot \rangle_{L^2(\Omega)}$ is obtained from (2) by setting $\ell = 0$. It is convenient to first obtain an expression for the L^2 gradient $\nabla^{L^2} \mathcal{J}_{\nu,\lambda}$ and then use identity (10) together with (2) to deduce the required Sobolev gradient $\nabla \mathcal{J}_{\nu,\lambda} = \nabla^{H^1} \mathcal{J}_{\nu,\lambda}$ [Protas *et al.*, 2004]. We note that the last term in expression (8) for the Gâteaux differential, $\mathcal{A}(\phi; \phi')$, is not consistent with the Riesz representation (10) since the arbitrary perturbation ϕ' does not appear in it explicitly as a linear factor and is instead "hidden" as the initial condition in the perturbation system (9). To transform this term to the required form, we use the adjoint calculus. Multiplying (9a) by the adjoint state $u^* : [0, T] \times \Omega \to \mathbb{R}$, integrating the resulting expression over $[0, T] \times \Omega$ and performing integration by parts with respect to t and x, we obtain

$$
0 = \int_0^T \int_0^{2\pi} \left(\frac{\partial u'}{\partial t} + u' \frac{\partial u}{\partial x} + u \frac{\partial u'}{\partial x} - \nu \frac{\partial^2 u'}{\partial x^2} \right) u^* \, dx \, dt
$$

$$
= \int_0^{2\pi} \left[u^*(T, x) u'(T, x) - u^*(0, x) u'(0, x) + \int_0^T \left(-\frac{\partial u^*}{\partial t} - u \frac{\partial u^*}{\partial x} - \nu \frac{\partial^2 u^*}{\partial x^2} \right) u' \, dt \right] dx,
$$
(11)

where all the boundary terms resulting from integration by parts in space vanish due to the periodic boundary conditions. Defining the adjoint system as

$$
-\frac{\partial u^*}{\partial t} - u \frac{\partial u^*}{\partial x} - \nu \frac{\partial^2 u^*}{\partial x^2} = 0 \qquad \text{in } (0, T] \times \Omega, \tag{12a}
$$

$$
u^*(t = T) = W(\phi) \qquad \text{in } \Omega, \tag{12b}
$$

with the terminal condition stated in Fourier space as

$$
\widehat{W}(k; \phi) = \begin{cases} -\frac{2\lambda}{\pi} \left[|\widehat{\phi}(k/\lambda)|^2 - \lambda \, |\widehat{u}(T, k; \phi)|^2 \right] \widehat{u}(T, k; \phi), & k = \lambda n, \qquad n \in \mathbb{N} \\ 0, & \text{otherwise} \end{cases}
$$
(13)

reduces (11) to

$$
\mathcal{A}(\phi; \phi') = \int_0^{2\pi} u^*(T, x) u'(T, x) \, dx = \int_0^{2\pi} u^*(0, x) \phi'(x) \, dx = \left\langle u^*(0, \cdot), \phi' \right\rangle_{L^2(\Omega)},
$$
(14)

where Parseval's theorem was used to express integrals of products of functions in terms of sums of products of their Fourier coefficients. The adjoint system

8

(12) is a terminal-value problem with the terminal condition (13) determined by the form of the Gâteaux differential (8), cf. (14), and hence also by the objective functional (5). Therefore, the system needs to be integrated backwards in time and its coefficients $u(t, x; \phi)$ are given by the solution of the governing system (1) around which linearization is performed.

Combining (8) and (14), we obtain the following expression for the L^2 gradient of the functional (5) given in terms of its Fourier-space representation as

$$\widehat{\nabla^{L^2} \mathcal{J}_{\nu,\lambda}}(k) = \frac{2}{\pi} \left[|\widehat{\phi}(k)|^2 - \lambda \, |\widehat{u}(T, \lambda k; \phi)|^2 \right] \widehat{\phi}(k) + \widehat{u}^*(0, k), \qquad k \in \mathbb{N}. \tag{15}$$

Since the L^2 gradient does not possess the regularity needed to construct solutions of Problem 1, we must determine the corresponding Sobolev H^1 gradient. Using the second equality in the Riesz identity (10) together with the definition (2) of the H^1 inner product, performing integration by parts and noting the arbitrariness of ϕ', we obtain the required H^1 gradient $\nabla \mathcal{J}_{\nu,\lambda}$ as a solution of the elliptic boundary-value problem

$$\left[\mathrm{Id} - \ell^2 \, \frac{\partial^2}{\partial x^2} \right] \nabla \mathcal{J}_{\nu,\lambda} = \nabla^{L^2} \mathcal{J}_{\nu,\lambda} \qquad \text{in } \Omega, \tag{16}$$

subject to the periodic boundary conditions. As shown in [Protas *et al.*, 2004], extraction of gradients in spaces of smoother functions such as $H^1(\Omega)$ can be interpreted as low-pass filtering of the L^2 gradients with the parameter ℓ acting as the cut-off length-scale.

The retraction operator in (7) is defined in terms of the normalization

$$\mathcal{R}_{\mathcal{S}}(\phi) := \sqrt{\frac{\mathcal{E}_0}{\mathcal{E}(\phi)}} \, \phi. \tag{17}$$

An optimal step size τ_n can be determined by solving the minimization problem

$$\tau_n = \underset{\tau > 0}{\arg \max} \left\{ \mathcal{J}_{\nu,\lambda} \left(\mathcal{R}_{\mathcal{S}} \left(\phi^{(n)} + \tau \, \nabla \mathcal{J}_{\nu,\lambda}(\phi^{(n)}) \right) \right) \right\}, \tag{18}$$

which can be interpreted as a modification of a standard line search problem [Nocedal and Wright, 2006] with optimization performed following an arc (a geodesic) lying on the constraint manifold $\mathcal{S}$, rather than a straight line. A numerical implementation of the approach described here is presented below.

3.1 Numerical Implementation

The governing system and the corresponding adjoint system, respectively (1) and (12), are discretized in space using a Fourier pseudo-spectral method. Nonlinear products are evaluated in physical space and appropriately dealiased using the 2/3 rule combined with a Gaussian filter introduced in [Hou, 2009]. Time integration is performed using a four-step, implicit/explicit Runge-Kutta scheme which yields globally third-order accuracy [Alimo *et al.*, 2020]. Since the number of spatial discretization points N and temporal step-size Δt heavily depend on the selected values of ν and λ, we defer the discussion of selection of these parameters to the next section. Nonetheless, validation of the gradient (15), which is a key element of the optimization approach and requires the numerical solution of both systems (1) and (12), is given in the Appendix A.

The Sobolev gradient is determined using $\ell = 10$ in (2) and the corresponding elliptic boundary-value problem (16) is solved using the Fourier-Galerkin spectral method. The line minimization problem (18) is solved using Brent's algorithm [Press *et al.*, 2007]. Iterations (7) were declared converged when a stopping criterion given in terms of the relative decrease of the cost functional, $|\mathcal{J}_{\nu,\lambda}(\phi^{(n)}) - \mathcal{J}_{\nu,\lambda}(\phi^{(n-1)})|/\mathcal{J}_{\nu,\lambda}(\phi^{(n-1)}) < 1 \times 10^{-8}$, was satisfied or the number of iteration exceeded the limit of $n = 1,000$. To accelerate convergence of the iterations in (7), the gradient $\nabla \mathcal{J}_{\nu,\lambda}\left(\phi^{(n)}\right)$ in (7) was replaced with a conjugate gradient constructed using the Polak-Ribière formula [Nocedal and Wright, 2006]. Our approach is implemented in MATLAB and the code is available in [Matharu].

4 Results

In this section we present results obtained by solving Problem 1 with $\mathcal{E}_0 = \pi$ and with λ and ν varying over a broad range of values, namely, $\lambda = 2, \ldots, 7$ and $\nu = 2.5 \times 10^{-3}, 2.5 \times 10^{-4}, 2.5 \times 10^{-5}, 2.5 \times 10^{-6}, 2.5 \times 10^{-7}$. We note that, with $\mathcal{E}_0$ fixed, decreasing the viscosity coefficient ν can be interpreted as increasing the "Reynolds number" of the flow. When λ increases and ν decreases, the numerical resolution both in space and in time needs to be refined in order for the solutions $u(t, x; \phi)$ to be well resolved, which can be checked by examining their Fourier spectra. The values of N and Δt used for different λ and ν are summarized in Table 1. As regards the choice of the time window T, our goal is for it to be on the order of an eddy turnover time (6), i.e., $T = C_T t_e$, where $C_T = \mathcal{O}(1)$. However, t_e depends on the solution $u(t, x; \varphi_{\nu,\lambda})$ of Problem 1 and therefore the actual value

of the constant C_T can only be determined a posteriori, i.e., after Problem 1 has been solved. Hence, in our computations we use a fixed time window $T = 0.6$ and the resulting values of the constant C_T are reported in Table 2. We have experimented with many other time windows T, both shorter and longer, and the results obtained were qualitatively similar to those reported below.

In order to illustrate the performance of algorithm (7), in Figure 1a we show the dependence of the objective functional $\mathcal{J}_{\nu,\lambda}(\phi^{(n)})$ on iterations n for the solutions of Problem 1 obtained with $\nu = 2.5 \times 10^{-5}$ and $\lambda = 2, 4, 6$. We see that the values of the objective functional drop significantly, down to $\mathcal{O}(10^{-8} - 10^{-9})$ with smaller values achieved for smaller λ. The expressions $f(k, \varphi_{\nu,\lambda})$, cf. (5), corresponding to the optimal solutions $\varphi_{\nu,\lambda}$ obtained for different λ are shown as functions of k in Figure 1b. We see that in all cases these expressions are generally decreasing functions of the wavenumber k.

Due to the nonlinearity of the governing system (1), Problem 1 is nonconvex and as such may admit multiple local minimizers. This is indeed the situation we encounter at least for some combinations of ν and λ. More specifically, we have found evidence for the existence of two distinct classes of solutions of Problem 1 that we refer to as *viscous* and *inertial*. Their main features are contrasted in Figure 2 and are summarized below.

- **Viscous solutions** involve highly oscillatory optimal initial conditions $\varphi_{\nu,\lambda}$, cf. Figure 2a, with energy concentrated at high wavenumbers k in the dissipative subrange, cf. Figure 2e. Consequently, the resulting evolution does not involve any inertial transfer of energy between different Fourier modes and instead the solutions are quickly attenuated by the viscous dissipation, cf. Figure 2c (which is the origin of the name we gave these solutions). The enstrophy $\mathcal{E}(u(t, \cdot; \varphi_{\nu,\lambda}))$ of viscous solutions is a rapidly decreasing function of time t, cf. Figure 2h. As they do not feature any large-scale structure and have a small magnitude, the viscous solutions resemble the minimizer $\phi_0 \equiv 0$ of functional (5) in the absence the constraint $\mathcal{E}(\phi) = \mathcal{E}_0 > 0$ (see the discussion before the statement of Problem 1).

- **Inertial solutions** minimize the objective functional (5) via inertial transfer of energy to Fourier modes with higher wavenumbers k, cf. Figure 2f, which in the physical space is achieved by a self-similar steepening of the wave fronts, cf. Figures 2b,d. As a result, the enstrophy $\mathcal{E}(u(t, \cdot; \varphi_{\nu,\lambda}))$ of inertial solutions is a rapidly increasing function of time t, cf. Figure 2h. In contrast to the viscous solutions, the magnitude of the inertial solutions does not change much over the time window T.

Viscous solutions are "generic" as they can be found by solving Problem 1 using essentially any initial guess ϕ_1. On the other hand, inertial solutions are "rare", in the sense that they can only be found if a "good" initial guess ϕ_1 is used in (7). The final values of the objective functional (5) are in both cases comparable, cf. Figure 1a, although the expressions $f(k, \varphi_{\nu,\lambda})$ tend to have a different dependence on k for the viscous and inertial solutions, cf. Figure 2g. Moreover, for a given value of λ the inertial solutions can only be found provided the viscosity coefficient ν is sufficiently small. This is because the inertial solutions involve a self-similar energy transfer between Fourier modes with wavenumbers k and λk, which can only happen if the inertial range is sufficiently wide or, equivalently, if the Reynolds number is sufficiently high. A key qualitative feature differentiating viscous and inertial solutions is the time evolution of the enstrophy (3) which is, respectively, a decreasing and an increasing function of time for these two families of solutions, cf. Figure 2h. Table 2 provides information about the values of λ for which inertial solutions could be found for decreasing values of ν, and also includes the number of wave fronts, P, present in the solution at the final time (during the evolution from $t = 0$ to $t = T$ this number typically decreases by no more than 15%). Needless to say, only the inertial solutions are self-similar in the sense of Definition 1 and hence we will exclusively focus on them in the remainder of this work.

We now examine how properties of the inertial solutions vary in function of the parameters ν and λ. Families of optimal initial conditions $\varphi_{\nu,\lambda}$ were obtained using a continuation approach where Problem 1 was solved for some ν_1 and λ_1 using either $\varphi_{\nu_2,\lambda_1}$ or $\varphi_{\nu_1,\lambda_2}$ for some $\mathbb{R}^+ \ni \nu_2 > \nu_1$ and $\mathbb{N}^+ \ni \lambda_2 < \lambda_1$ as the initial guess ϕ_1 in (7). The solutions found for fixed viscosity coefficients ν and increasing values of λ are summarized in Table 3, where we see that when $\lambda > 2$ inertial solutions can be found only provided ν is sufficiently small. The reason for this is clear when we examine the Fourier spectra of the optimal initial conditions $\varphi_{\nu,\lambda}$ and of the corresponding final states $u(T, \cdot; \varphi_{\nu,\lambda})$ (the third and fourth columns in Table 3) — we see that during its evolution the solution develops a well-defined inertial range where energy is cascaded in a self-similar manner minimizing the objective functional (5). When the viscosity is large, this inertial range does not persist long enough to accommodate energy transfer between Fourier coefficients with a large separation in the wavenumber space, which needs to happen when λ is large.

In terms of the physical-space representation, the self-similar energy cascade is realized by the steepening of the wave fronts which is clearly visible in the first and second columns of Table 3. In other words, during the evolution over

$[0, T]$ the global structure of the solutions remains essentially unchanged, but all the wave fronts steepen in almost the same manner. There are some apparent similarities in how this process unfolds in solutions obtained with even and odd values of λ. When ν is fixed, the number of distinct fronts in the solution is an increasing function of λ which is illustrated in Figure 3. Table 2 provides more details about this trend, although additional data would be needed in order to determine the precise form of the dependence of P on λ for a fixed ν. Finally, in Table 4 we characterize solutions obtained by solving Problem 1 with $\lambda = 2, 5$ and different values of ν (this is a subset of the results already shown in Table 3, but organized in a different manner). We see that, interestingly, both the optimal initial conditions $\varphi_{\nu,\lambda}$ and the corresponding final states $u(T, x; \varphi_{\nu,\lambda})$ appear to converge to well-defined limits as $\nu \to 0$ while their Fourier spectra become more developed.

| λ / ν	2	3	4	5	6	7
2.5×10^{-3}	$N = 4096$ $\Delta t = 1 \times 10^{-3}$	$N = 8192$ $\Delta t = 1 \times 10^{-3}$	$N = 8192$ $\Delta t = 1 \times 10^{-3}$	$N = 16384$ $\Delta t = 1 \times 10^{-3}$		
2.5×10^{-4}	$N = 8192$ $\Delta t = 5 \times 10^{-4}$	$N = 16384$ $\Delta t = 5 \times 10^{-4}$	$N = 16384$ $\Delta t = 5 \times 10^{-4}$	$N = 32768$ $\Delta t = 5 \times 10^{-4}$	$N = 65536$ $\Delta t = 5 \times 10^{-4}$	$N = 65536$ $\Delta t = 5 \times 10^{-4}$
2.5×10^{-5}	$N = 16384$ $\Delta t = 5 \times 10^{-4}$	N=131072 $\Delta t = 2 \times 10^{-4}$	N=131072 $\Delta t = 2 \times 10^{-4}$	N=131072 $\Delta t = 2 \times 10^{-4}$	N=131072 $\Delta t = 2 \times 10^{-4}$	N=131072 $\Delta t = 2 \times 10^{-4}$
2.5×10^{-6}	$N = 16384$ $\Delta t = 5 \times 10^{-4}$					
2.5×10^{-7}	$N = 16384$ $\Delta t = 5 \times 10^{-4}$					

Table 1: The number of spatial discretization points N and the temporal step size Δt used to solve Problem 1 for different values of the parameters ν and λ. Pink background in a cell indicates that no inertial solutions were found for the given values of ν and λ. If a cell is left blank, then no attempt was made to solve Problem 1 with the corresponding values of ν and λ.

ν \ λ	2	3	4	5	6	7
2.5×10^{-3}	$C_T = 0.70$ $P = 9$	$C_T = 0.09$	$C_T = 0.09$	$C_T = 0.21$		
2.5×10^{-4}	$C_T = 0.75$ $P = 10$	$C_T = 0.81$ $P = 19$	$C_T = 0.85$ $P = 15$	$C_T = 0.72$ $P = 27$	$C_T = 0.51$	$C_T = 0.53$
2.5×10^{-5}	$C_T = 0.75$ $P = 10$	$C_T = 1.44$ $P = 19$	$C_T = 0.90$ $P = 20$	$C_T = 1.35$ $P = 28$	$C_T = 0.67$ $P = 40$	$C_T = 0.86$ $P = 48$
2.5×10^{-6}	$C_T = 0.74$ $P = 10$					
2.5×10^{-7}	$C_T = 0.74$ $P = 10$					

Table 2: Values of the constant $C_T = T/t_e$ relating the optimization time window T and the eddy turnover time t_e, cf. (6), for different values of ν and λ. In addition, for inertial solutions, we show the number of wave fronts P present in the solution at final time. Pink background in a cell indicates that no inertial solutions where found for the given values of ν and λ (and hence P was not determined). If a cell is left blank, then no attempt was made to solve Problem 1 with the corresponding values of ν and λ.
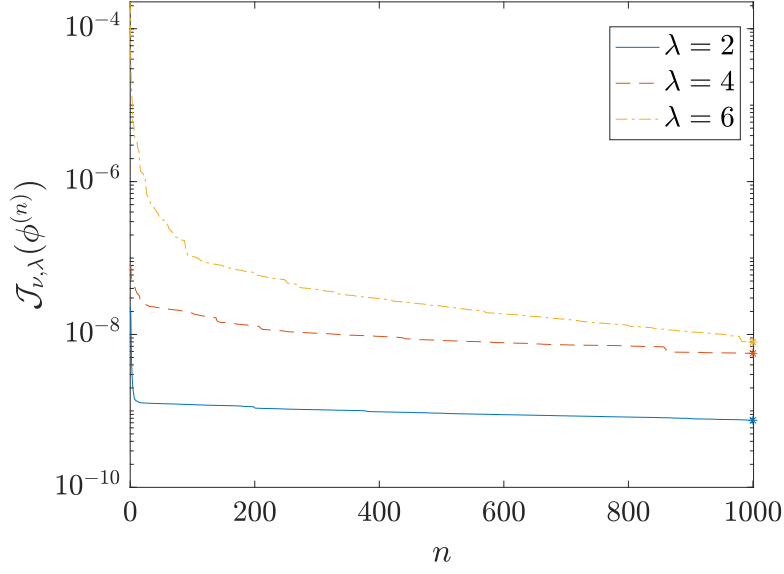
(a)
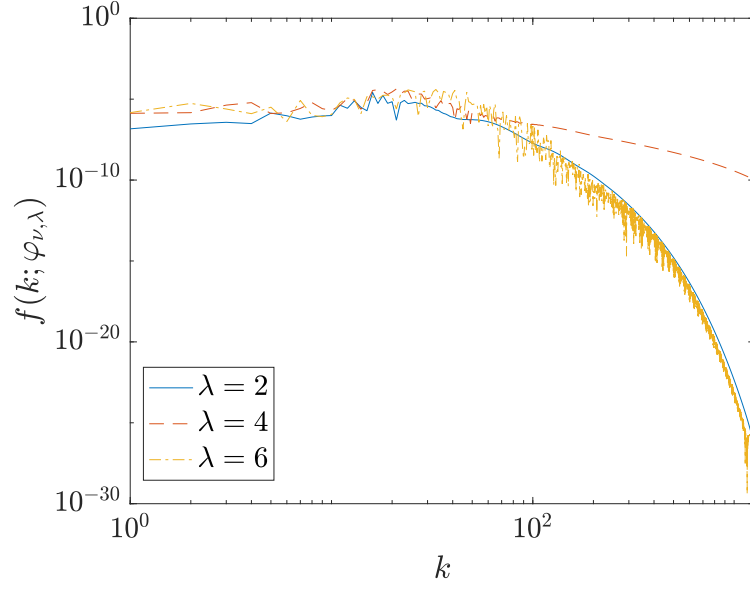
(b)

Figure 1: (a) Decrease of the objective functional (5) with iterations n and (b) the corresponding distributions $f(k; \varphi_{\nu,\lambda})$ obtained at the minima when solving Problem 1 with $\nu = 2.5 \times 10^{-5}$ and (blue solid line) $\lambda = 2$, (red dashed line) $\lambda = 4$, and (yellow dot-dashed line) $\lambda = 6$.
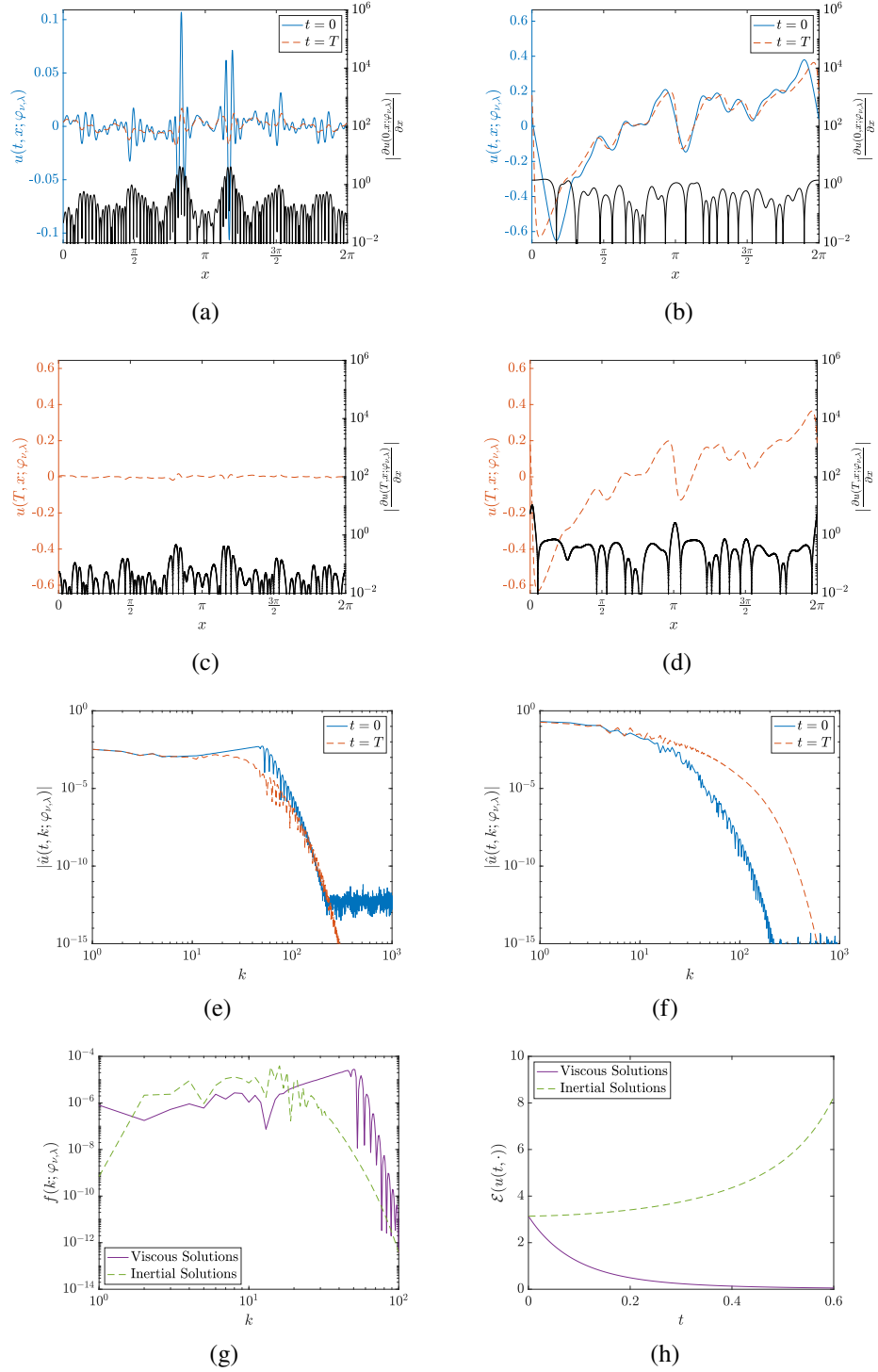
Figure 2: Comparison of the properties of (left column) the viscous solutions and (right column) the inertial solutions obtained by solving Problem 1 with $\nu = 2.5 \times 10^{-3}$ and $\lambda = 2$: (a,b) optimal initial conditions $\varphi_{\nu,\lambda}(x)$ (blue, left axis), the magnitude of their gradients $|d\varphi_{\nu,\lambda}(x)/dx|$ (black, right axis) and the corresponding solutions $u(T, x; \varphi_{\nu,\lambda})$ at the final time (red, left axis); (c,d) the solutions at the final time $u(T, x; \varphi_{\nu,\lambda})$ (red, left axis) and their gradients $|\partial u(T, x; \varphi_{\nu,\lambda})/\partial x|$ (black, right axis); (e,f) the Fourier spectra $\widehat{\varphi_{\nu,\lambda}}(k)$ (blue) and $\widehat{u}(T, k; \varphi_{\nu,\lambda})$ (red) of the optimal initial conditions and of the corresponding final states; (g, h) the functions $f(k; \varphi_{\nu,\lambda})$ vs. k and $\mathcal{E}(u(t, \cdot; \varphi_{\nu,\lambda}))$ vs. t, cf. (5) and (3), respectively, at the minimum for the viscous solution (purple) and the inertial solution (green).
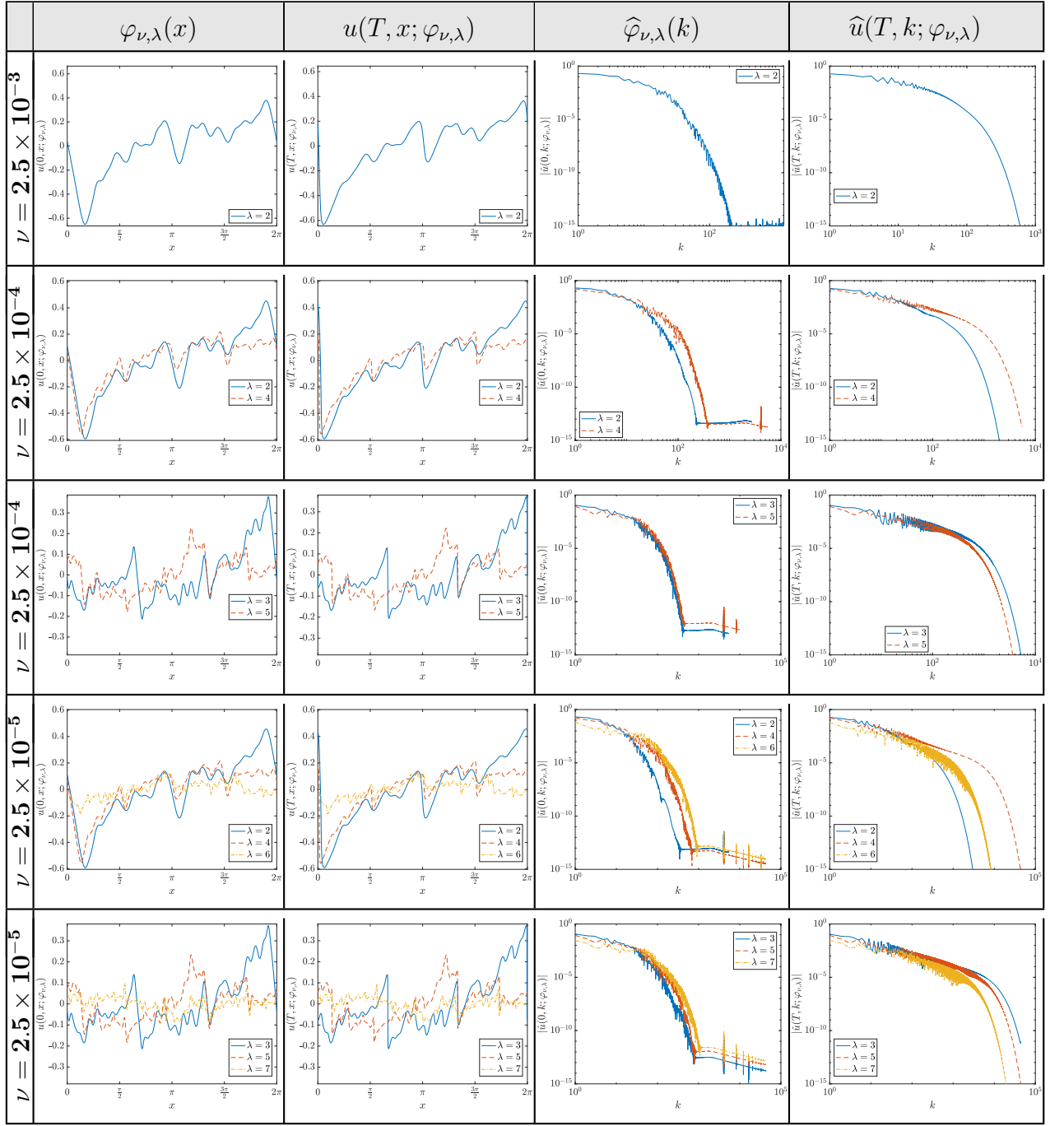
Table 3: Summary information about the inertial solutions found by solving Problem 1 with the values of ν indicated on the left and the values of λ given in the individual legends. For a better comparison the solutions obtained with even and odd λ are grouped together. The first and the second columns represent the optimal initial conditions $\varphi_{\nu,\lambda}$ and the final states $u(T, x; \varphi_{\nu,\lambda})$, with the corresponding spectra given in the third and fourth columns.
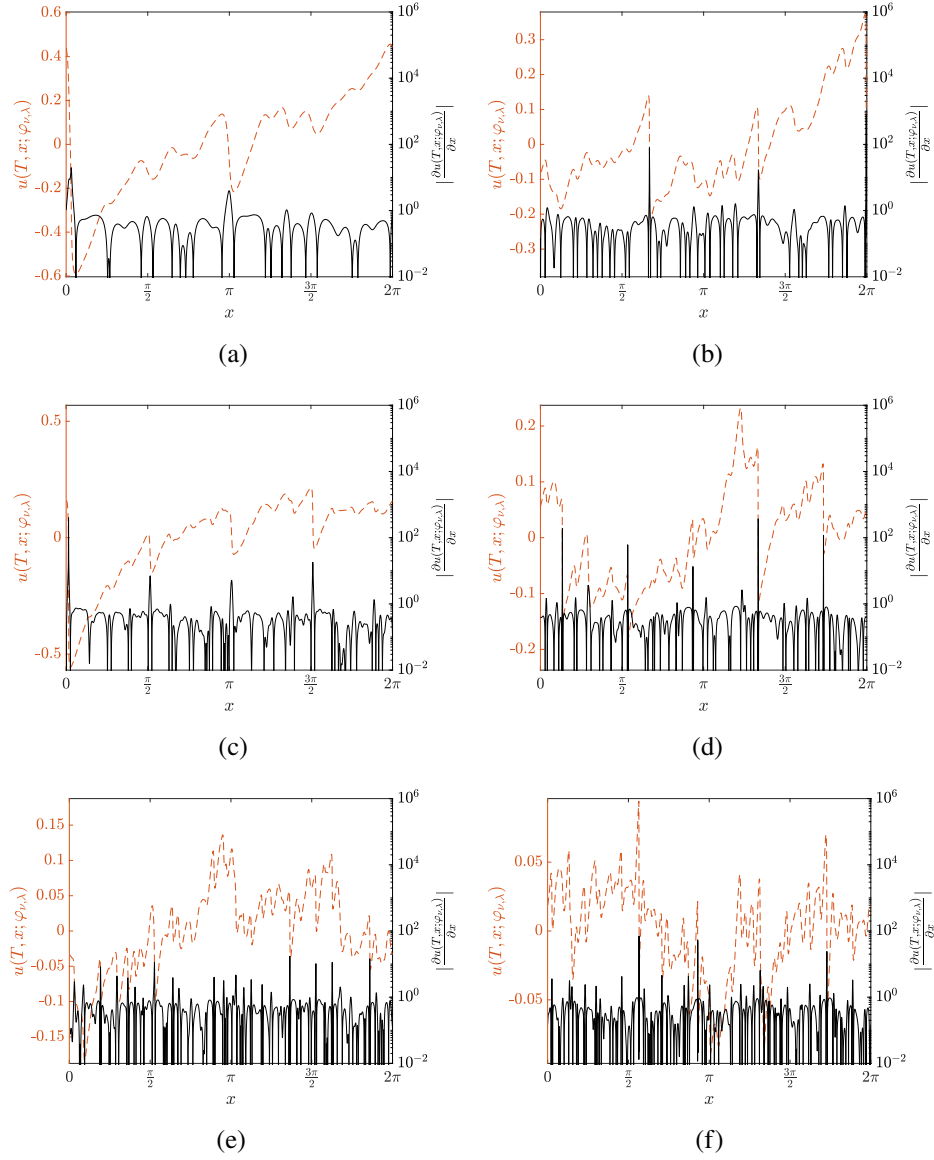
	$\varphi_{\nu,\lambda}(x)$	$u(T,x;\varphi_{\nu,\lambda})$	$\widehat{\varphi}_{\nu,\lambda}(k)$	$\widehat{u}(T,k;\varphi_{\nu,\lambda})$
$\lambda=2$				
$\lambda=5$				
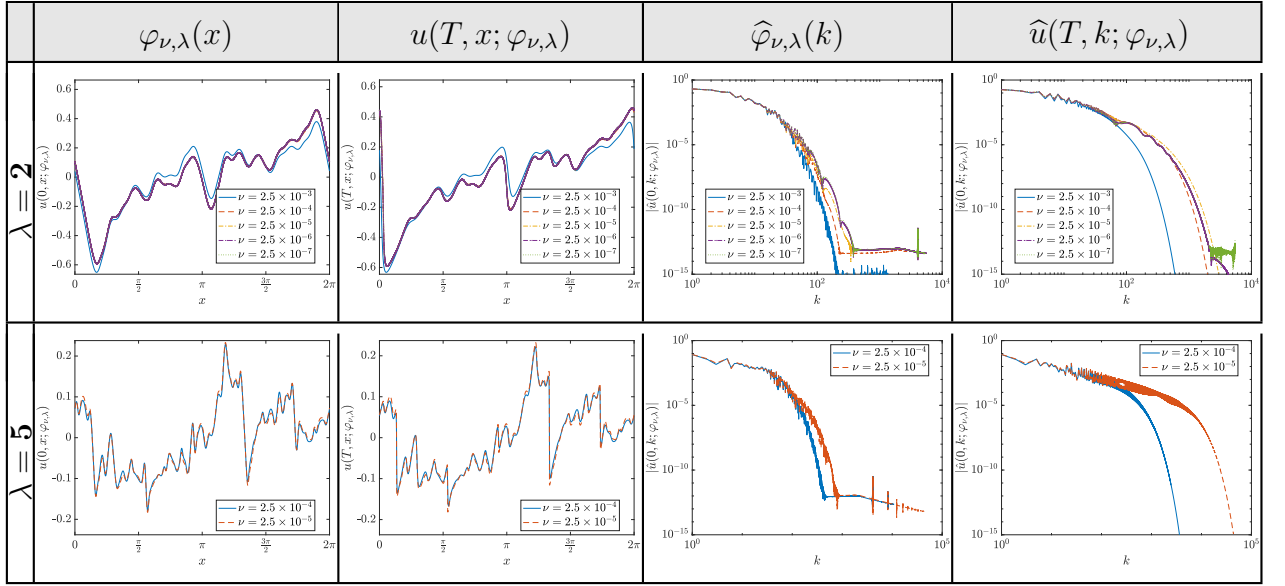
Table 4: Summary information about the inertial solutions found by solving Problem 1 with $\lambda = 2$ (top row) and $\lambda = 5$ (bottom row), and different values of ν indicated in the individual legends. The first and the second columns represent the optimal initial conditions $\varphi_{\nu,\lambda}$ and the final states $u(T,x;\varphi_{\nu,\lambda})$, with the corresponding spectra given in the third and fourth columns.

19

Figure 3: Solutions at the final time $u(T, x; \varphi_{\nu,\lambda})$ (red, left axis) and their gradients $|\partial u(T, x; \varphi_{\nu,\lambda})/\partial x|$ (black, right axis)) obtained by solving Problem 1 with $\nu = 2.5 \times 10^{-5}$ and (a) $\lambda = 2$, (b) $\lambda = 3$, (c) $\lambda = 4$, (d) $\lambda = 5$, (e) $\lambda = 6$, and (f) $\lambda = 7$.

20

5 Conclusions

This study was motivated by an open question in turbulence research concerning the nature of fluid motions that can give rise to a self-similar energy cascade as predicted by Kolmogorov's statistical theory of turbulence [Kolmogorov, 1941, Frisch, 1995]. While the real problem concerns flows in 3D, here we consider a simple toy model, namely, the 1D viscous Burgers equation, and provide a proof of concept for a novel approach to this problem, where solutions with a self-similar structure consistent with Definition 1 are constructed systematically. This is done by solving a family of PDE optimization problems, cf. Problem 1, where we seek initial conditions for system (1) such that deviations from the self-similar behavior are minimized by the corresponding flow evolution over a period of time approximately equal to one eddy turnover time (6). This somewhat nonstandard PDE optimization problem is solved numerically for different values of ν and λ using a state-of-the-art adjoint-based gradient method described in Section 3. The optimal solutions $\varphi_{\nu,\lambda}$ found in this way correspond to very small values of the objective functional (5), cf. Figure 1a, indicating that they satisfy Definition 1 of self-similarity down to numerical approximation and round-off errors.

The solutions found fall into two distinct categories referred to as viscous and inertial distinguished by the behavior of the enstrophy $\mathcal{E}(u(t, \cdot; \varphi_{\nu,\lambda}))$ which, respectively, decays and grows in these types of solutions, cf. Figure 2h. The former solutions are uninteresting as they consist of high-wavenumber oscillations in the viscous subrange of the Fourier spectrum and as such are quickly attenuated by viscous dissipation without producing any significant energy transfer across scales. Therefore, they resemble the trivial solution $\phi_0 \equiv 0$ of the corresponding unconstrained problem, with the high-wavenumber oscillation added to satisfy the constraint $\mathcal{E}(\phi) = \mathcal{E}_0$. The fact that such physically uninteresting, yet mathematically consistent, solutions have been found demonstrates the robustness of algorithm (7).

On the other hand, the inertial solutions lead to flow evolutions involving a self-similar, in the sense of Definition 1, transfer of energy in the Fourier space, which in the physical space is manifested by a uniform steepening of the wave fronts, cf. Table 3 and Table 4. As expected, optimal solutions involving such energy transfer over a large distance in the Fourier space can only be found provided the viscosity ν is sufficiently small (or, equivalently, the "Reynolds number" is sufficiently large). Interestingly, the structure of these self-similar solutions is preserved as $\nu \to 0$, cf. Table 4, suggesting that it might persist in the limiting inviscid problem (for times before the inviscid solutions become singular).

21

To the best of our knowledge, the results reported here represent the first successful effort to construct time-dependent solutions of a hydrodynamic model characterized by self-similar energy transfer. Both the viscous and inviscid Burgers equations are in principle analytically solvable [Kreiss and Lorenz, 2004] and it is an interesting open question whether this fact could be used to rigorously justify the results presented here. While in this study we focused on a toy problem, the results obtained show promise for this approach to be applied to real turbulent flows governed by the 3D Navier-Stokes system, an effort which is already underway. In addition, an analogous problem could also be considered in the context of two-dimensional flows.

A   Validation of Gradient (15)

In order to validate the computation of gradient (15), which is obtained by solving the adjoint system (12) with the rather nonstandard terminal condition (13) using the numerical approach described in Section 3.1, we compute the Gâteaux (directional) differential (8) in two ways: in terms of an approximation using a first-order forward finite difference formula with the step size ϵ and in terms of the Riesz formula (10) involving the gradient $\nabla^{L^2} \mathcal{J}_{\nu,\lambda}(\phi)$. The ratio of these two quantities is thus defined as

$$\kappa(\epsilon) := \frac{\epsilon^{-1} \left[\mathcal{J}_{\nu,\lambda}(\phi + \epsilon\phi') - \mathcal{J}_{\nu,\lambda}(\phi) \right]}{\left\langle \nabla^{L^2} \mathcal{J}_{\nu,\lambda}(\phi), \phi' \right\rangle_{L^2(\Omega)}}, \qquad \epsilon > 0, \tag{19}$$

where $\phi, \phi' \in L^2(\Omega)$ represent, respectively, the "point" where the Gâteaux differential is computed and the direction. Given the equivalence of the Riesz representations involving the L^2 and H^1 inner products, cf. (10), for simplicity we choose to use the former in the denominator of (19).

For intermediate values of ϵ the dominant errors come from the discretization of systems (1) and (12), and are independent of ϵ; we thus expect that $\kappa(\epsilon) \to 1$ as the discretization is refined, i.e., as $N \to \infty$ and $\Delta t \to 0$. On the other hand $\kappa(\epsilon)$ will deviate from 1 for both small and large ϵ due to, respectively, the subtractive cancellation (round-off) errors and the truncation errors in the finite-difference formula, both of which are well known effects. A detailed discussion of the interplay between these different types of errors is given in [Matharu and Protas, 2024, Figure 2].

To fix attention, in the tests reported here, we set $T = 0.6$, $\nu = 2.5 \times 10^{-3}$ and $\lambda = 2, 7$, and use the initial condition $\phi(x) = -\sin(x)$. Since integration in time is usually the main source of errors when employing pseudospectral methods in space, Figure 4 shows that indeed $\kappa(\epsilon) \to 1$ for intermediate $\epsilon \in [10^{-10}, 10^{-5}]$ as the temporal discretrization Δt is refined with a fixed spatial resolution of $N = 16, 384$ and two different perturbations ϕ'. Similar trends were also observed in tests performed with other values of T, ν and λ (not shown here for brevity). This thus demonstrates the consistency of the computation of the gradient $\nabla^{L^2} \mathcal{J}_{\nu,\lambda}(\phi)$, both in terms of the derivation of the adjoint system (12)–(13) and the numerical implementation.
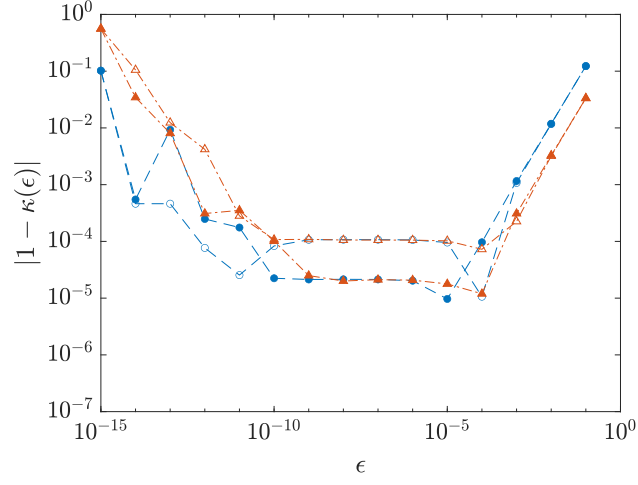
(a)
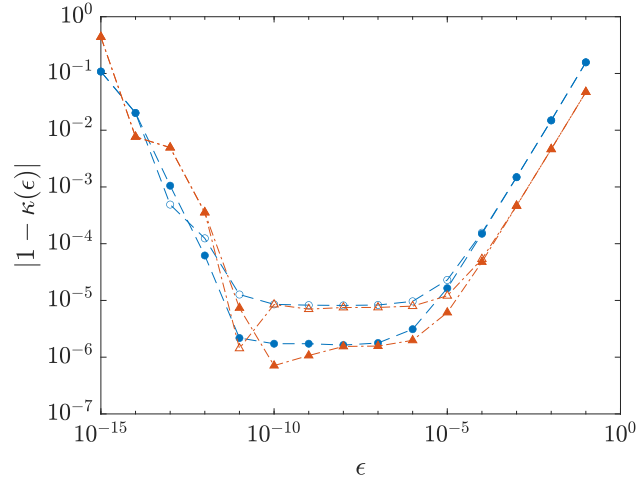
(b)

Figure 4: Dependence of $|\kappa(\epsilon) - 1|$ on ϵ for (a) $\lambda = 2$ and (b) $\lambda = 7$. Expression (19) was evaluated using the temporal discretizations (empty symbols) $\Delta t = 1 \times 10^{-3}$ and (filled symbols) $\Delta t = 2 \times 10^{-4}$, and the perturbations (blue circles) $\phi' = \sin(-x)$ and (red triangles) $\phi' = \frac{1}{2+\sin(x)}$.

24

Acknowledgements

References

U. Frisch, *Turbulence*, 1st ed. (Cambridge University Press, Cambridge, 1995).

L. F. Richardson, *Weather prediction by numerical process* (Cambridge University Press, Cambridge, UK, 1922).

A. Kolmogorov, Dokl. Akad. Nauk SSSR **30**, 9 (1941), (translated and reprinted 1991 in Proc. R. Soc. Lond. A **434**, 9–13).

S. Goto, Y. Saito, and G. Kawahara, Phys. Rev. Fluids **2**, 064603 (2017).

T. Yoneda, S. Goto, and T. Tsuruhashi, Nonlinearity **35**, 1380 (2022).

T. Tsuruhashi, S. Goto, S. Oka, and T. Yoneda, Phil. Trans. R. Soc., A **380**, 20210053 (2022).

M. D. Gunzburger, *Perspectives in Flow Control and Optimization* (SIAM, 2003) https://epubs.siam.org/doi/pdf/10.1137/1.9780898718720 .

A. Jameson, Journal of Scientific Computing **3**, 233 (1988).

T. R. Bewley, P. Moin, and R. Temam, Journal of Fluid Mechanics **447**, 179 (2001).

P. Matharu and B. Protas, SIAM J. Sci. Comput. **42**, B250 (2020), https://doi.org/10.1137/19M1251941 .

P. Matharu and B. Protas, Phys. Rev. Fluids **7**, 044605 (2022).

B. Protas, Philosophical Transactions of the Royal Society A: Mathematical, Physical and Engineering Sciences **380**, 20210035 (2022).

D. Ayala and B. Protas, Physica D **240**, 1553 (2011).

D. Ayala, C. R. Doering, and T. M. Simon, Journal of Fluid Mechanics **837**, 839 (2018).

R. R. Kerswell, C. C. T. Pringle, and A. P. Willis, Reports on Progress in Physics **77**, 085901 (2014).

P. Matharu, B. Protas, and T. Yoneda, Physica D: Nonlinear Phenomena **441**, 133517 (2022).

D. Ayala and B. Protas, Journal of Fluid Mechanics **818**, 772 (2017).

D. Kang, D. Yun, and B. Protas, Journal of Fluid Mechanics **893**, A22 (2020).

D. Kang and B. Protas (2021), arXiv:2110.06130.

X. Zhao and B. Protas, Journal of Nonlinear Science **33**, 1 (2023).

P. Hassanzadeh, G. Chini, and C. Doering, Journal of Fluid Mechanics **751**, 627–662 (2014).

C. J. Miles and C. R. Doering, Journal of Nonlinear Science **28**, 2153 (2018).

H. Kreiss and J. Lorenz, *Initial-Boundary Value Problems and the Navier-Stokes Equations*, Classics in Applied Mathematics, Vol. 47 (SIAM, 2004).

R. Adams, *Sobolev Spaces* (Academic Press, New York, 2003).

J. Bec and K. Khanin, Phys. Rep. **447**, 1 (2007).

J.-D. Fournier and U. Frisch, J. Méc. Théor. Appl. **2**, 699 (1983).

D. Pelinovsky, Proceedings of Royal Society A **468**, 3636 (2012a).

D. Pelinovsky, Dynamics of Partial Differential Equations **9**, 305 (2012b).

D. Albritton and N. D. Nitti, Nonlinearity **36**, 7142 (2023).

B. P. Murray and M. D. Bustamante, Journal of Fluid Mechanics **850**, 624 (2018).

M. Buzzicotti, B. P. Murray, L. Biferale, and M. D. Bustamante, The European Physical Journal E **39**, 34 (2016).

B. Protas, D. Kang, and M. D. Bustamante, Phys. Rev. E **109**, 055104 (2024).

P.-A. Absil, R. Mahony, and R. Sepulchre, *Optimization Algorithms on Matrix Manifolds* (Princeton University Press, 2008).

M. S. Berger, *Nonlinearity and Functional Analysis* (Academic Press, 1977).

B. Protas, T. R. Bewley, and G. Hagen, J. Comp. Phys. **195**, 49 (2004).

J. Nocedal and S. Wright, *Numerical Optimization*, 2nd ed., Springer Series in Operations Research and Financial Engineering (Springer, 2006) pp. xxii+664.

T. Y. Hou, Acta Numer. **18**, 277 (2009).

R. Alimo, D. Cavaglieri, P. Beyhaghi, and T. R. Bewley, J. Glob. Optim. 10.1007/s10898-019-00855-1 (2020).

W. H. Press, S. A. Teukolsky, W. T. Vetterling, and B. P. Flannery, *Numerical recipes*, 3rd ed. (Cambridge University Press, 2007) pp. xxii+1235, the art of scientific computing.

P. Matharu, Self-Similar Energy Tranfer for 1D Burgers Equation (BurgersEnergyTransfer) (2025)., URL https://github.com/pipmath/BurgersEnergyTransfer.

P. Matharu and B. Protas, J. Comput. Phys. **517**, 113298 (2024).